4-1-2004

Relative timing of substorm onset phenomena

L. Kepko

M. G. Kivelson

R. L. McPherron

Harlan E. Spence
Boston University, harlan.spence@unh.edu

Recommended Citation

Kepko, L., M. G. Kivelson, and R. L. McPherron (2004), Relative timing of substorm onset phenomena, J. Geophys. Res., 109, A04203, doi:10.1029/2003JA010285.

Relative timing of substorm onset phenomena

L. Kepko
Center for Space Physics, Boston University, Boston, Massachusetts, USA

M. G. Kivelson and R. L. McPherron
Institute of Geophysics and Planetary Physics, University of California, Los Angeles, Los Angeles, California, USA

H. E. Spence
Center for Space Physics, Boston University, Boston, Massachusetts, USA

Received 10 October 2003; revised 7 January 2004; accepted 28 January 2004; published 2 April 2004.

[1] In this paper we examine the temporal ordering of midtail flow bursts, Pi2 pulsations, and auroral arc brightening at substorm onset. We present three substorm events for which the Geotail spacecraft was situated at local midnight, near the inner edge of the plasmasheet. We show that high-speed, convective Earthward directed plasma flows observed by Geotail occurred 1–3 min before auroral onset as observed by the Polar Visible Imaging System and Ultraviolet Imager auroral imagers on board the Polar spacecraft. We also show that the onsets of both nightside Pi2 pulsations and magnetic bay variations were simultaneous with auroral onset. We argue that these observations lend strong support to the flow burst-driven model of magnetotail dynamics. We also examine a high-latitude magnetic precursor to onset and show that it is likely due to the currents expected from the passage of a flow burst through the plasmasheet prior to substorm onset. Finally, we calculate an analytic expression for this current and show that it is unlikely to generate discrete auroral structures. *INDEX TERMS:* 2788 Magnetospheric Physics: Storms and substorms; 2704 Magnetospheric Physics: Auroral phenomena (2407); 2740 Magnetospheric Physics: Magnetospheric configuration and dynamics; 2744 Magnetospheric Physics: Magnetotail; 2708 Magnetospheric Physics: Current systems (2409); *KEYWORDS:* substorm, Pi2 pulsations, bursty bulk flows (BBFs), aurora

Citation: Kepko, L., M. G. Kivelson, and R. L. McPherron (2004), Relative timing of substorm onset phenomena, *J. Geophys. Res.*, *109*, A04203, doi:10.1029/2003JA010285.

1. Introduction

[2] The relative ordering of the various magnetospheric substorm onset phenomena (e.g., auroral arc brightening, Pi2 pulsations, geosynchronous dipolarization, etc.) has been the focus of intense debate since the auroral substorm was formally defined by *Akasofu* [1964]. Two viable onset mechanisms for the initiation of a substorm (see reviews by *Baker et al.* [1996] and *Lui* [1996]) have emerged over the subsequent four decades of research. In one scenario reconnection is thought to begin slowly on closed field lines in the middle magnetotail ($X \sim = -20$ to $X \sim = -30\ R_E$) until lobe field lines are reached. With the accompanying jump in Alfvén speed, the reconnection rate increases dramatically. A high-speed flow burst of several hundreds of km/s travels earthward, and the impact of the flow burst upon the inner magnetosphere then generates the substorm current wedge, auroral arc brightening, and Pi2 pulsations [*Birn et al.*, 1999; *Shiokawa et al.*, 1998]. The other possibility is that the instability associated with onset occurs in the near-Earth region, near the transition between stretched tail and dipolar field lines [e.g., *Lui*, 1996]. There are several competing near-Earth models, differing mainly by the instability that disrupts the current, and they are collectively referred to as near-geosynchronous onset (NGO) models. The rapid dipolarization caused by the disruption of the near-Earth cross-tail current creates a tailward propagating rarefaction wave which forces the tail current sheet over the instability threshold, initiating magnetic reconnection. Auroral arc brightening in the NGO scenario would precede flows in the middle magnetotail, and perhaps Pi2 pulsations as well, by several (1–3) minutes [*Liou et al.*, 2000]. Because the two scenarios for substorm onset predict a different sequence of observable events, precise determination of the relative timing of the different onset phenomena is of vital importance. In practice, however, establishing the temporal ordering of onset phenomena has been difficult because of the small differences in timing involved and the relative lack of relevant spacecraft coverage.

[3] Nonetheless, the International Solar-Terrestrial Physics (ISTP) era brought unprecedented spatial coverage of the regions of the magnetosphere affected by substorms. Motivated by the wealth of ISTP data, a wide array of studies were undertaken to establish the temporal and causal relationships of onset phenomena. Most of these studies

0148-0227/04/2003JA010285

have examined the relative timing of just two phenomena with respect to one another. For example, *Nagai and Machida* [1998] found that flow bursts in the middle magnetotail preceded low-latitude Pi2 pulsations by 1–3 min. A separate study by *Liou et al.* [2000] found that auroral arc brightening also preceded low-latitude Pi2 pulsations by 1–3 min. Together, these studies suggest that auroral onset and the initiation of high-speed midtail plasma flows are simultaneous which, if correct, would suggest a near-Earth onset mechanism. However, intercomparison of statistical studies can be subject to errors because different criteria for selecting onset times are often used. For example, as *Kepko and McPherron* [2001] pointed out, the *Liou et al.* [2000] study used differing criteria for auroral onset and Pi2 onset, which artificially introduced the 1–3 min delay. When comparable criterion were used, auroral arc brightening and nightside Pi2 were observed to occur simultaneously, within the resolution of the auroral imagery data.

[4] Ideally, comprehensive event studies can provide an overall picture of substorm onset timing. Such studies have been hindered by the lack of ideal conjunctions of spacecraft. For example, while one can often identify auroral substorm onset in Polar VIS or UVI auroral data, orbital realities and the sheer size of the magnetotail limit the number of auroral events in which Geotail, for example, is favorably located to observe the onset of substorm-associated flow. In this paper we present three events in which spacecraft and ground stations were fortuitously located in favorable positions to determine accurately the relative temporal ordering of substorm expansion phase onset phenomena. We show that flow bursts preceded the auroral and ground signatures by ~1–3 min, and that nightside Pi2 and arc brightening were virtually simultaneous. We also present evidence of a high-latitude, magnetic precursor to auroral onset and Pi2 pulsations. We then examine the observed ordering with respect to the two primary onset theories, and conclude that the flow-driven model of magnetospheric dynamics better explains the observations. Finally, we develop an analytic expression relating the earthward motion of a magnetotail flow burst to the high-latitude Pi2 precursor.

2. Events

[5] The events described here were previously presented by *Kepko et al.* [2001] as examples of the correlation between the waveforms of midtail flow bursts and low-latitude, flank Pi2. In that study we showed that the flow bursts preceded ground Pi2 onset by several minutes, and that the flow bursts directly drove low-latitude, flank Pi2. Here we include global auroral imagery from the Visible Imaging System (VIS) [*Frank et al.*, 1995] and the Ultraviolet Imager (UVI) [*Torr et al.*, 1995] on board the Polar spacecraft and we further refine the temporal relationship of substorm onset phenomena. Throughout this paper, UVI images are displayed in geomagnetic coordinates, while the VIS images are displayed without geographic registration. Data from a wide array of spacecraft and ground stations are used in this study. Data from the geomagnetic tail are exclusively from Geotail. The Geotail magnetic field data are from the MGF experiment [*Kokubun et al.*, 1994] and are in GSM coordinates and are sampled at 12-s resolution. Geotail plasma moments are from the LEP experiment [*Mukai et al.*, 1994] and are also at 12-s resolution. Velocity data are in GSM coordinates. In addition, we have used ground magnetometer data from a variety of stations. The 210 magnetic meridian (MM) stations span an area covering Eastern Russia and Western Australia to Hawaii [*Yumoto et al.*, 1996]. Data are typically sampled at 1-s resolution. The Canopus array spans Canada and magnetic field data are at 5-s resolution. We also present data from the Los Alamos station of the UCLA/IGPP network.

2.1. September 4, 1997

[6] For this first event Geotail was located at (−9.8, 0.6, 0.1) R_E in GSM coordinates. The positions of Geotail and the ground stations that we will use in our analysis are shown in Figure 1. Ewa (Ewa Beach, λ_{mag} = 21.3 N, φ_{mag} = 202.0 E), a nearly equatorial station from the 210°MM magnetometer network, was located in the pre-midnight sector, and the station's position has been mapped along dipole field lines to the GSM equatorial (Z = 0) plane. Daw (Dawson, λ_{mag} = 64.1° N, φ_{mag} = 220.9° E), from the Canopus magnetometer chain, was located near the footprint of Geotail. For the 30 min prior to the event the *AL* index was never larger than approximately −30 nT, indicating that the magnetospheric activity was quite low. The event onset (at 0948 UT) was followed by a rapid 80 nT drop in the *AL* index and ~45 min later by the onset of a large substorm. We concern our analysis with the first onset at 0948 UT. While the size and duration of this first bay variation would not be termed a substorm, we will show that phenomena characteristic of substorms were observed during the event.

2.1.1. Auroral Observations

[7] Images recorded by the Ultraviolet Imager (UVI) and the Visible Imaging System (VIS) on board the Polar spacecraft are shown in Figure 2. The UVI images alternate between pairs taken in the Lyman-Birge-Hopfield long (LBHL) and short (LBHS) wavelength bands. Each pair consists of an 18-s integrated image and a 36-s integrated image. The smearing of auroral features in each image from lower left to upper right is due to spacecraft wobble. The image taken during 0947:59-0948:17 UT is the first to show an enhanced auroral arc, which was then observed to brighten further and expand slightly. Subsequent images show that the arc faded significantly in intensity after 0951 UT. This is consistent with the auroral electrojet indices which showed that this event was of short duration. The VIS images, shown in the bottom half of Figure 2, were integrated over 55-s. A brightening is observed in the 0947:53-0948:48 UT image, consistent with the time determined from the UVI images. Of note is the 0946:53-0947:48 UT image taken during a small gap in the UVI images, which shows no auroral enhancement. On the basis of the combined UVI and VIS observations, we confidently place the auroral onset time between 0947:59 and 0948:17.

2.1.2. Timing

[8] The magnetic field and velocity moments from Geotail are shown in Figure 3. The large value of B_x relative to B_z near 0945 UT suggests that Geotail was initially located near the outer edge of the plasmasheet. As the event progressed, the spacecraft found itself located progressively

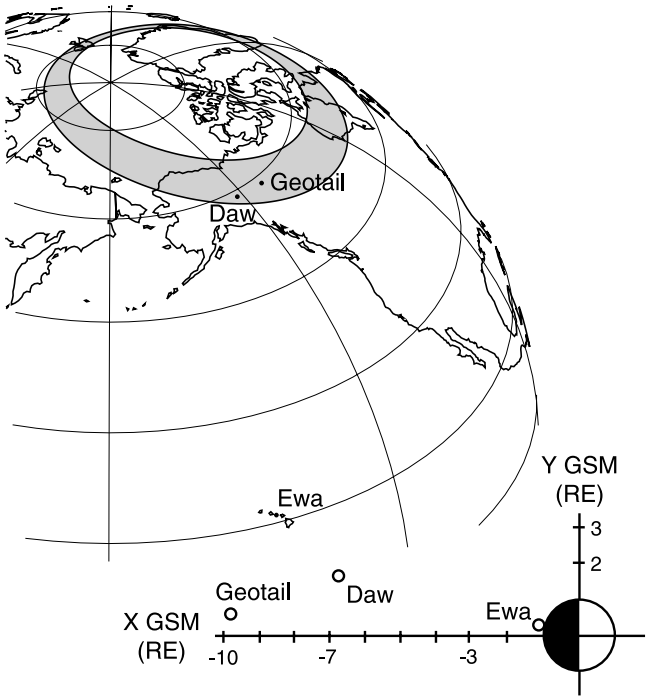

Figure 1. The locations of Geotail and the ground stations Dawson (Daw) and Ewa Beach (Ewa) for the September 4, 1997 event. The positions of the ground stations have been mapped along field lines to the GSM equatorial plane (below), and the position of Geotail has similarly been mapped to the ground (above).

closer to the central plasma sheet. In Figure 3b we show the X component of the perpendicular ion flow velocity ($v_{\perp}\hat{x}$), which increased to ~200 km/s at 0947:09 UT, indicating the onset of convective, earthward flow. Oscillations with Pi2 (~1–2 min) periodicity are evident from 0947–0953 UT. During the interval of high-speed flow the B_z component of the field increased by ~5 nT. Between major flow bursts short periods of tailward flow were observed, the largest of which occurred after the last flow burst at 0952:30 UT. These tailward flows were likely caused by relaxation of the flux tubes earthward of the flows. Several of the bursts exhibited a negative V_z component (not shown). Geotail was located in the southern half of the plasma sheet during the event, and an earthward flow originating in the central plasma sheet would have a southward component as the flow diverged along field lines.

[9] Magnetic field data from Ewa Beach of the 210°MM magnetometer network and Dawson of the Canopus magnetometer chain are shown in Figure 3c. Magnetic oscillations started at Ewa just after 0948 UT, approximately 1 min after the start of similar oscillations in the flow velocity at Geotail. The waveforms of the earthward component of the perpendicular flow velocity measured at Geotail ($v_{\perp}\hat{x}$), shifted by +60s, and the X component of the magnetic field measured at Ewa are quite similar over the first three cycles. As we have previously shown, the low-latitude Pi2 were directly driven by the variations in the earthward flow [*Kepko et al.*, 2001].

[10] We also show in Figure 3c the three components of the magnetic field in geographic coordinates (XYZ) from Dawson, which was located near the magnetic footpoint of Geotail. In this coordinate system, X points north, Y points east and Z points down. Just after 0948 UT Dawson, at much higher latitude than Ewa Beach but near the same local time, observed the sharp onset of a negative bay created by an increase in the magnitude of the current flowing in the westward electrojet. The UVI images indicated the brightening of an auroral arc at about this same time (gray box in Figure 3). This is an important observation, and as we will show for the other events, nightside Pi2, the formation of the substorm current wedge and auroral arc onset are simultaneous, within the resolution of the auroral measurements.

[11] Prior to the high-latitude onset observed at Dawson at 0948 UT, small perturbations in both the X and Z components of the magnetic field were observed. A gradual decrease in the X component began at 0945 UT, and the Z component began to increase gradually about 2 min later. We believe this precursor to Pi2 pulsations and the negative bay was related to the motion of the flow burst through the magnetotail. We discuss later in this paper how this movement could generate ionospheric currents that produce the magnetic perturbations.

2.2. July 22, 1998

[12] This next event occurred early on July 22, 1998. Geotail was located at (−9.0, 0.3, 0.8) R_E in GSM coordinates. The mapped locations of the ground stations and Geotail are shown in Figure 4. Both auroral imagery and auroral indices indicate that magnetospheric activity was quite low before the onset of a moderate substorm near 0700 UT. The AL index reached a minimum of −200 nT ~ 45 min later. For this event we had near perfect sun-earth alignment of Geotail and the ground stations Island Lake (Isl) and Los Alamos (Lanl), which provides excellent constraints on both the direction of signal propagation and the time of flight. In addition, the 210°MM stations were located on the dayside. These stations observed Pi2 pulsations significantly delayed relative to the nightside Pi2.

2.2.1. Auroral Observations

[13] Images recorded by the Ultraviolet Imager (UVI) and Visible Imaging System (VIS) on board the Polar spacecraft are shown in Figure 5. Alternation of images from UVI is as for Figure 2. The first, faint indication of brightening in the UVI images occurred in the 0656:01-0656:19 UT image, appearing near 23 LT and 65° magnetic latitude. This arc was observed to brighten further and expand poleward in the successive images. Images from the VIS were integrated over 48 s, with a 6-s gap between successive images. The first brightening in the VIS data occurred in the 0655:06-0655:54 UT image, during a gap in the UVI data coverage. We note that the previous VIS image coincided with two UVI images. None of the images show any enhancement. The brightening in the 48-s VIS image at 0655:06-0655:54 UT is minor. The next UVI image also shows a minor brightening, so it seems likely that the auroral onset occurred just prior to 0656 UT. We take the entire VIS interval, 0655:30 ± 24s UT, as the auroral onset time.

2.2.2. Timing

[14] The plasma flow velocity from Geotail is also shown in Figure 5. An interval of high-speed flow was first detected at Geotail near 0654 UT. As in the previous event,

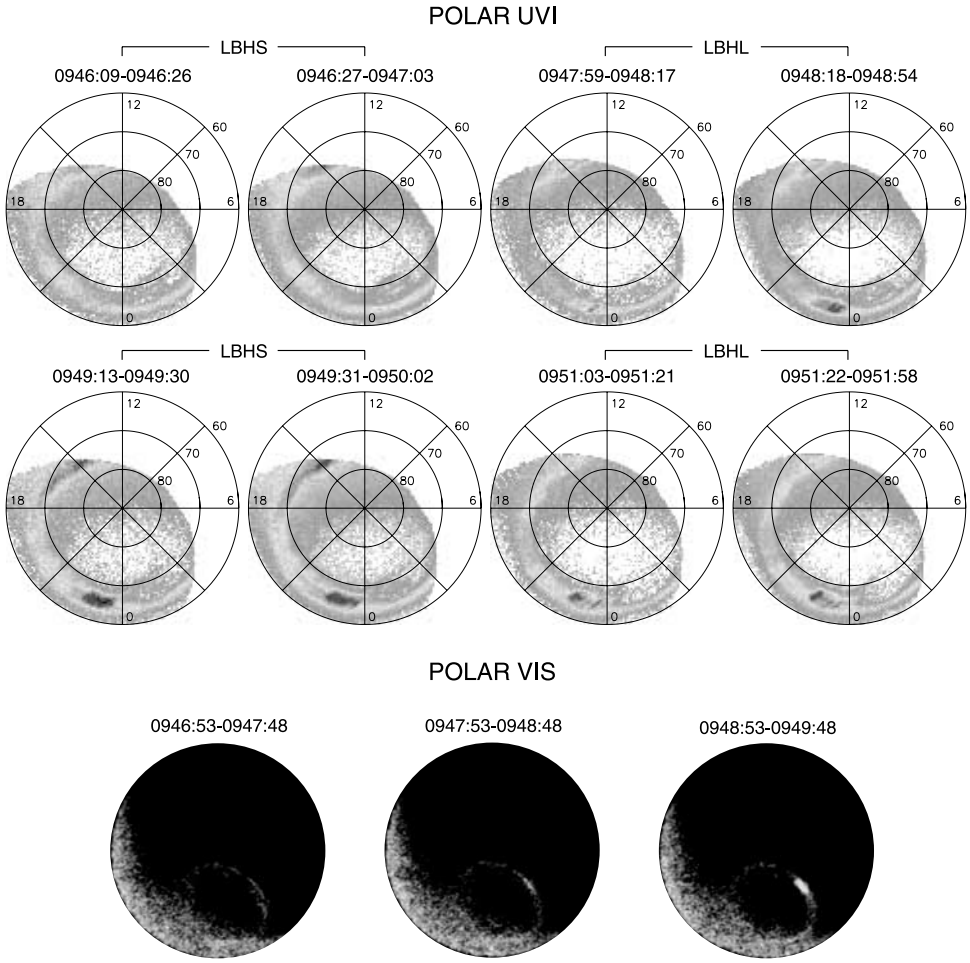

Figure 2. Images from the Polar UVI (rows 1 and 2) and VIS (row 3) for the September 4, 1997 event. The first indication of auroral brightening is observed in the 0947:59-0948:17 UVI image. Later images show that this arc intensifies and expands. In all VIS images, diffuse brightness at latitudes equatorward of the auroral oval occurs in sunlit regions and identifies dayside local times. See color version of this figure at back of this issue.

the Geotail velocity data show highly variable flow with oscillations in the Pi2 frequency band. The magnetic field data (Figure 6b) indicate that Geotail was in the center of the plasma sheet for the duration of the event, as B_x was relatively small. B_z increased by almost 20 nT as the magnetic field dipolarized. The dipolarization started almost simultaneously with the first flow burst which indicates that Geotail was located in the braking region. This is consistent with the Geotail location at $X = -9\ R_E$ GSM. After each of the first three velocity bursts the flow direction reversed briefly, indicating that the plasma was moving tailward. Following the third burst between 0659 and 0701 UT the flow remained negative. Despite this, we have shown that the perturbations during this interval were associated with ground Pi2 perturbations on the ground [*Kepko et al.*, 2001]. The negative velocity between earthward flow bursts suggests that the flow coming in from the tail had momentarily stopped, and the inner magnetosphere, compressed because of the dynamic pressure imposed by the flow burst, relaxed and moved outward.

[15] In Figure 6 we show the X component of the flow velocity from Geotail, the vertical component of the magnetic field from Geotail, and the magnetic field from several ground stations. The shaded bar corresponds to the time of integration of the image from the VIS that first showed auroral onset (0655:06-0655:54 UT). The first indication of change in any of the measurements is an increase in the earthward component of the bulk flow velocity at the position of Geotail beginning near 0654:05 UT (Figure 6a, first vertical line). The next indication of activity is a slight negative deflection in the X component of the high-latitude station Gil (Gillam, λ_{mag} = 63.9° N, φ_{mag} = 336.2° E), at around 0655 UT (Figure 6c, second vertical line). This deflection increased smoothly into the Pi2 pulsations and negative bay. The midlatitude Lanl station (Los Alamos λ_{mag} = 44.6° N, φ_{mag} = 318.0° E), located near the same magnetic longitude as Gil, did not observe the initial deflection (Figure 6d). Instead, it detected an abrupt onset of Pi2 pulsations and a small positive bay starting at 0655:30 UT (Figure 6d, third vertical line). These same pulsations were observed at high-latitude as well (with a 180 phase difference), indicating that there is no propagation delay between the two stations. This correlation confirms that the precursor observed by the Gil station prior to Pi2 pulsations was related to a localized current at high-latitude. *Kepko et al.* [2001] suggested that the Pi2 observed

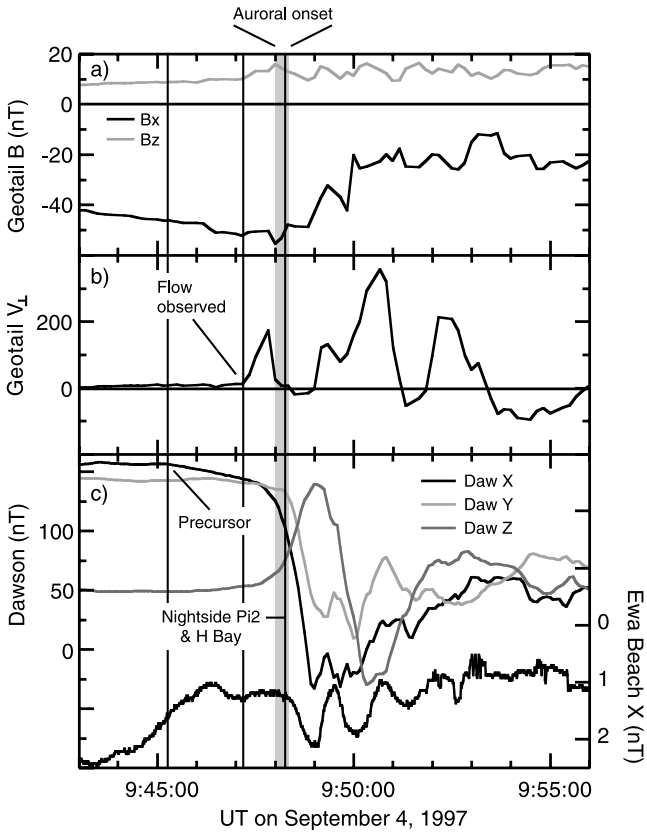

Figure 3. a) The X and Z components of the magnetic field and b) the perpendicular X component of the plasma flow velocity observed by Geotail. c) The three components of the magnetic field measured at Dawson, and the X component of the magnetic field measured at Ewa Beach. The start of the Pi2 precursor is indicated by the first vertical line. The first indication of enhanced convective flow observed at Geotail is marked by the second vertical black line, while the start of Pi2 pulsations at Ewa and the negative bay at Dawson is indicated by the third vertical line. Auroral onset determined by the UVI imager is indicated by the gray box.

by Lanl were examples of inertial current Pi2 that were directly associated with the currents generated by flow braking. Low-latitude stations on the flank (Figure 6e) also observed Pi2 pulsations, starting just before 0656 UT (fourth vertical line). This was ~20–30 s after pulsations were observed at Gillam and Los Alamos.

[16] It is clear from Figure 6 that the start of midlatitude Pi2 pulsations, the midlatitude positive bay, and auroral arc brightening occurred simultaneously, within the resolution of the auroral images. There was a precursor at high-latitudes on the nightside prior to any Pi2 or auroral signature. Earthward flow at $X = -9$ R_E was observed ~90 s before any ground or ionospheric onset phenomena.

2.3. October 26, 1997

[17] The positions of the ground stations and Geotail are shown in Figure 7. Geotail was located at (−13.6, 0.3, −1.2) R_E in GSM coordinates. The 210° MM array spanned the pre-midnight sector while the Canopus magnetometer array spanned the area between midnight and dawn. Polar UVI and VIS images indicate that this was a minor breakup. Auroral indices were not available, but Dawson of the Canopus magnetometer array was located near the breakup and detected a small (30 nT) negative bay consistent with the auroral imagery.

2.3.1. Auroral Observations

[18] Images from the Polar UVI (top) and VIS (bottom) are shown in Figure 8, along with the X component of the plasma velocity from Geotail. The UVI on board Polar was imaging at wavelengths of 1304 and 1356 in addition to the standard LBHL and LBHS wavelengths. As in the previous events, each wavelength is imaged twice, first with an 18-s integration followed by a 36-s integration. The auroral images for this event highlight some of the problems inherent in using global auroral images from space to identify auroral onset. We define "auroral onset" in the usual way as the time of formation of discrete auroral structures. Naked eye and all-sky observations of the auroral substorm indicate that dim, diffuse auroral arcs are present for up to tens of minutes prior to onset. Indeed, these quiescent arcs were included in the *Akasofu* [1964] definition of the auroral substorm. When either one or more of these arcs or a newly formed arc intensifies above an arbitrary threshold we state that an auroral substorm onset has occurred. This threshold can vary depending upon the sensitivity of the instrument, integration time, and wavelength of observation, but the associated uncertainty of timing is small because the change from the pre-substorm state occurs over a very short time-scale and is usually,

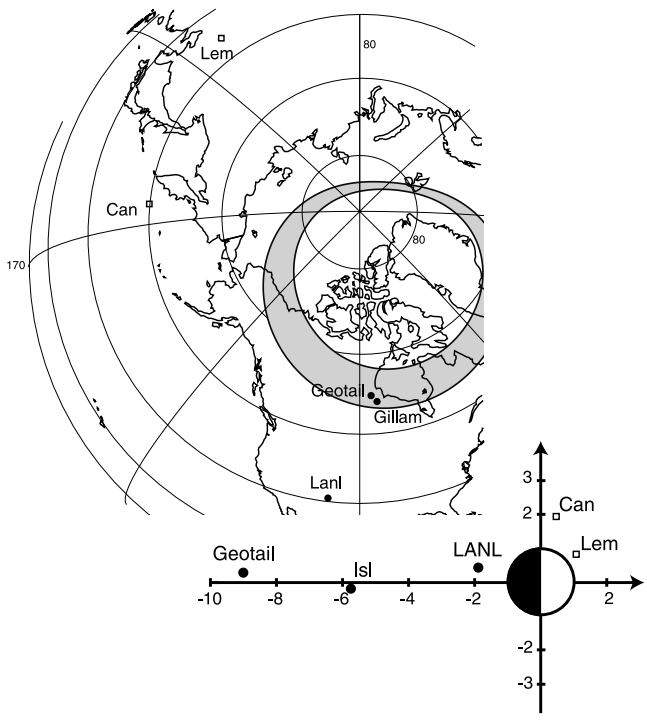

Figure 4. As for Figure 1 but for event at 0650 UT on July 22, 1998. The conjugate points for the southern hemisphere stations Can and Lem are shown. Locations of the spacecraft and the ground stations in the $Z = 0$ GSM plane. Stations have been mapped along field lines determined by the *Tsyganenko* [1989] model.

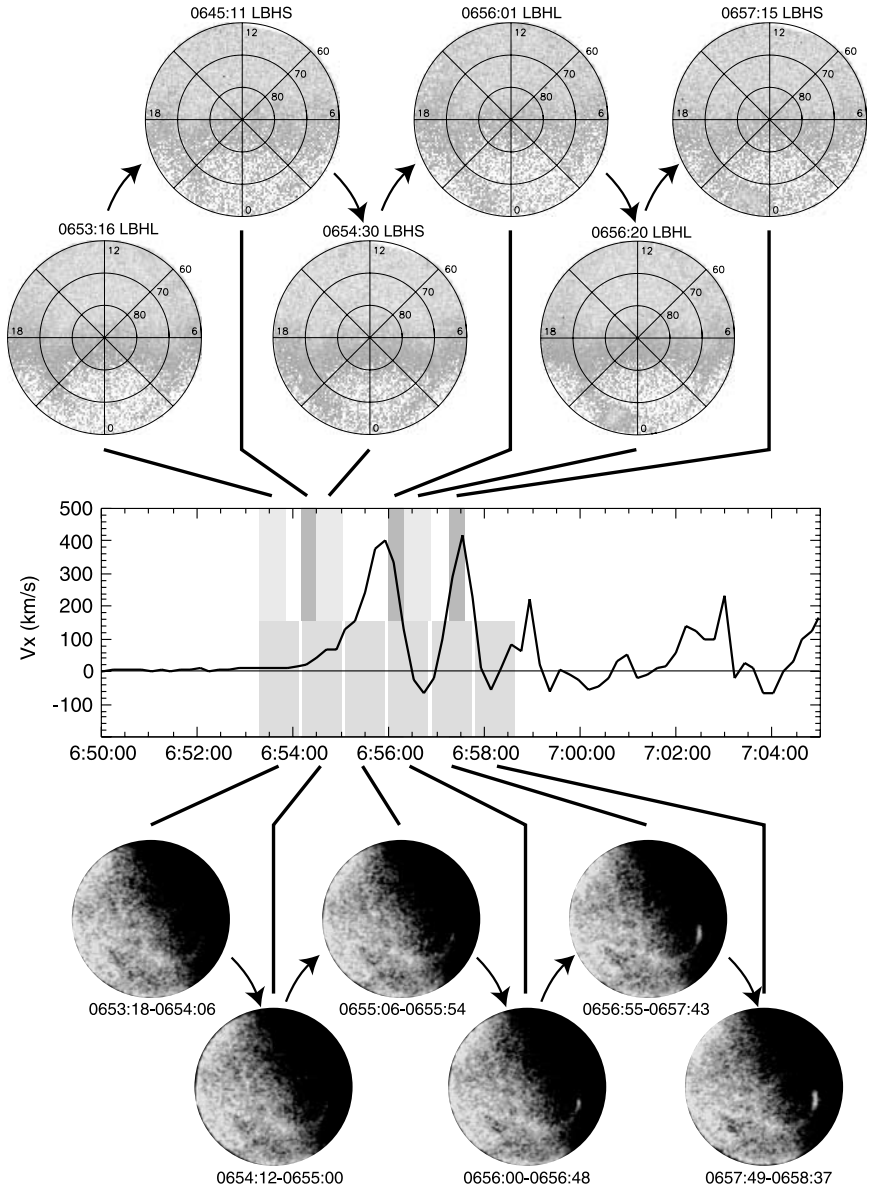

Figure 5. Auroral images from the UVI (top) and VIS (bottom) from Polar for the July 22, 1998, event. Detailed descriptions of the images are given in the text. Also shown (middle) are the flow data from Geotail. Shaded boxes indicate integration periods for each image. See color version of this figure at back of this issue.

though not always, quite dramatic. This facilitates easy identification of auroral substorm onset, and is the primary reason why ''auroral onset'' is typically used interchangeably with ''substorm onset''. For this event, however, we will show that the time of auroral onset is difficult to determine precisely through visual inspection of VIS and UVI imagery.

[19] Because the definition of auroral onset differentiates between diffuse, quiet-time arcs and discrete arcs it is important to have instrumentation that has the ability to observe and discriminate between different types of auroral structures. In this regard, we are aided by the Polar imagers. The VIS images the aurora near the edge of the visible spectrum. Because of the relatively low photon energy at these wavelengths, VIS can often detect diffuse auroral structures. In contrast, the UVI was designed to capture the higher-energy photons emitted by precipitating particles with energies associated with the discrete aurora. The UVI images are therefore a more discriminating indicator of what we and others term ''auroral onset''. As we will show auroral onset is clearly captured in the UVI images whereas the VIS images show a more gradual increase in auroral intensity. The timing obtained from the VIS images is therefore more ambiguous. Because of differing sensitivities between the filters of the UVI, comparison of intensities in the auroral images must make use of images of the same wavelength and integration time. For example, comparison of the 1127:13 LBHL image to the 1128:08 UT LBHS image initially suggests that an arc brightened near local midnight in the time between the images (Figure 8). However, the 18-s LBHS image of 1122 UT (Figure 9b) indicates that the arc was previously present at that wavelength, well before substorm onset. The first clear indication of brightening in the UVI images is in the 1130:56 UT 1304 image. There

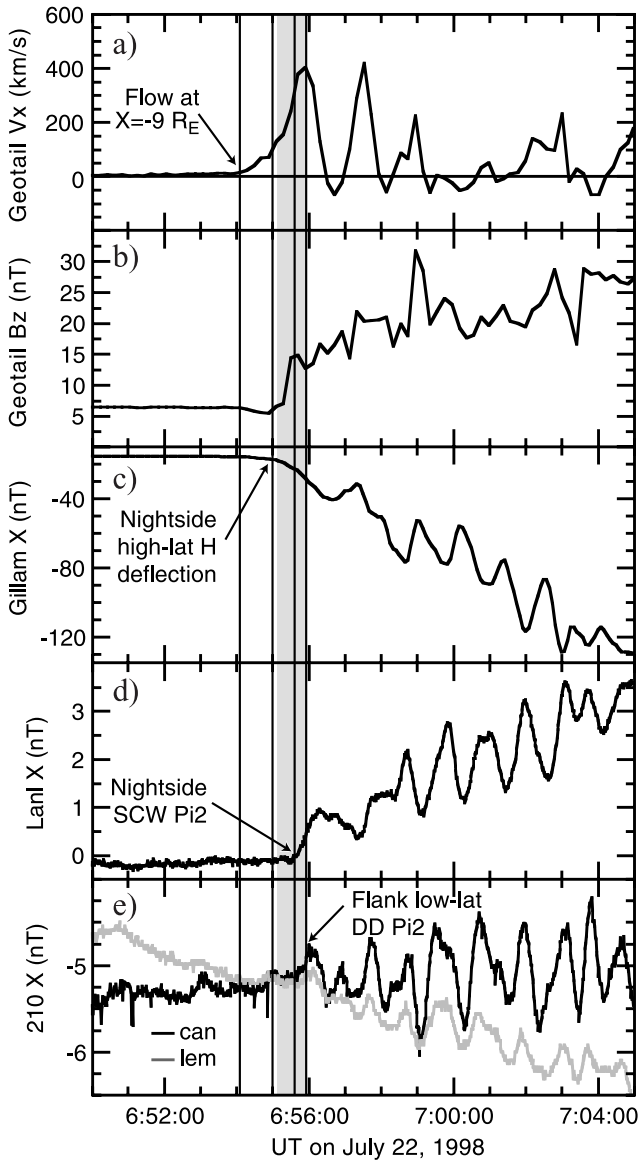

Figure 6. Timing of the July 22, 1998 event. In order from the top, Geotail first detected the start of high-speed flow at 0654:05 UT (first vertical line), followed by a small negative deflection at Gil (second vertical line), midlatitude Pi2 pulsations at Lanl (third vertical line), and finally low-latitude Pi2 (fourth vertical line). Shading shows the range of time within which auroral onset occurred.

appears to be some brightening in the 18-s 1304 image taken immediately prior to that, but comparison with the previous 18-s 1304 image taken 6 min earlier shows only minor differences (Figure 9a). The timing of auroral onset determined from the VIS data is even more ambiguous. A clear brightening is observed in the 1130:55-1131:46 UT image, which is in agreement with the UVI image of 1130:54-1131:30 UT. The overlapping UVI and VIS images are consistent with the interpretation that discrete auroral structures formed just after 1130:50 UT, near the end of the 1130:35-1130:53 UT UVI image and at the beginning of the 1130:55-1131:46 VIS UT image. There is a minor, localized bright region in the 1129:55-1130:46 UT VIS image, but despite the 51-s integration time, the intensity is not high, and the change from the previous image is minimal. The plasma flow velocity data from Geotail are also shown in Figure 8. As with the previous event, the Polar UVI and VIS auroral image integration intervals are identified. A large, variable flow burst lasting ~6 min started just after at 1128 UT, although flow at <100 km/s preceded this for ~90 s. Although uncertainties in the auroral imagery preclude the determination of an exact onset time, we can state with certainty that intensification of the auroral structures did not occur until at least 2 min after the first detection of high-speed ion flow by Geotail.

2.3.2. Timing

[20] The relative timing of the onset signatures may be seen in Figure 10, where we plot the magnetic field data from the ground stations of the Canopus magnetometer array and the 210° MM array, in addition to the Geotail measurements. Figure 10a shows the X component of the convective flow velocity ($V_{\perp}\hat{x}$) measured at Geotail, and a vertical line marks the onset of high-speed Earthward flow at 1128:15 UT. The magnetic field was highly variable during the interval of high-speed flow, and there was significant B_z transport (Figure 10b). The post-flow magnetic field did not show an appreciable change in B_z. This is consistent with the change in **B** expected at the position of Geotail, which was located too far downtail ($X = -13.6\ R_E$) to observe flux pile-up at such an early stage of substorm expansion. Geotail might have observed dipolarization if the substorm had developed further [*Baumjohann et al.*, 1999]. Compare, for example, with the July 22, 1998 event in Figure 6, where Geotail was located at $X = -9\ R_E$.

[21] The high-latitude stations Daw, Sim (Fort Simpson, λ_{mag} = 67.4° N, φ_{mag} = 300.6° E) and Isl (Island Lake, λ_{mag} = 61.4° N, φ_{mag} = 336.4° E) from the Canopus magnetometer array were located on the nightside (see

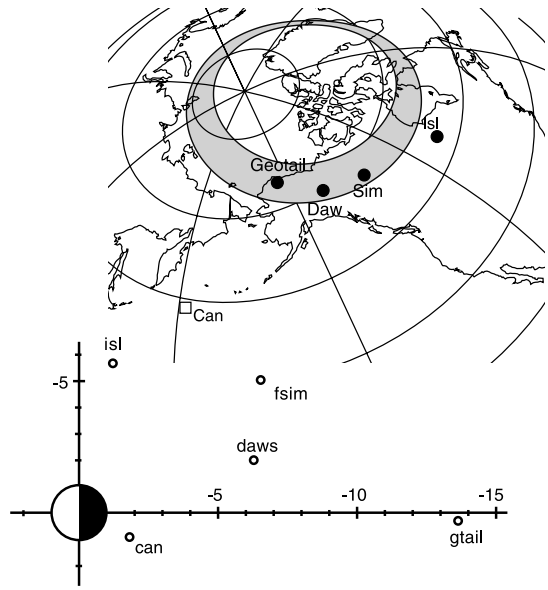

Figure 7. As for Figure 1 for the October 26, 1997, event. The conjugate points are shown for the southern hemisphere stations Can and Lem.

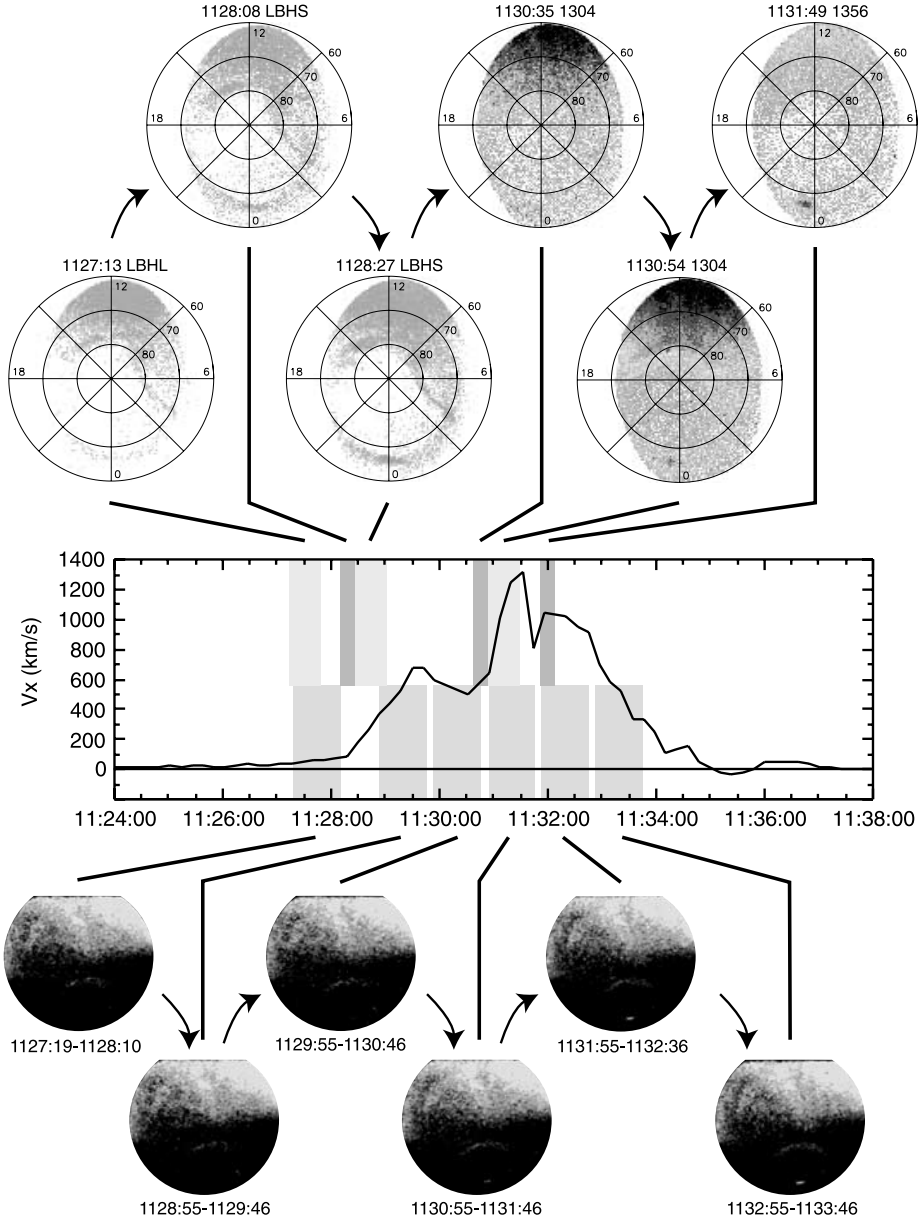

Figure 8. Images from the Polar UVI (top) and VIS (bottom) auroral imagers for the October 26, 1997, event. Also shown (middle) are the flow data from Geotail. Shaded boxes identify integration periods for each auroral image. See color version of this figure at back of this issue.

Figure 7) and observed a decrease in the X component starting at 1126 UT, prior to the initiation of high-speed flow at the location of Geotail and before the beginning of Pi2 pulsations on the ground a few minutes later. At Isl, which was located closer to the dawn meridian, the deflection was weak. The high-latitude deflection continued to increase gradually until 1131:30 UT, when the slope changed sharply, especially at Daw (second vertical line in Figure 10). This

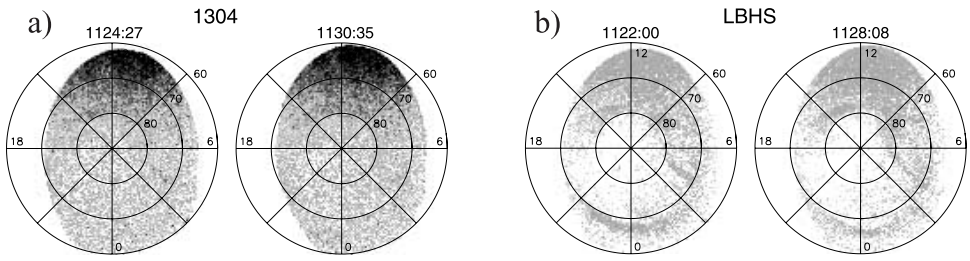

Figure 9. Comparison of pairs of a) 1304 and b) LBHS images taken ~6 min apart by the UVI on board Polar. See color version of this figure at back of this issue.

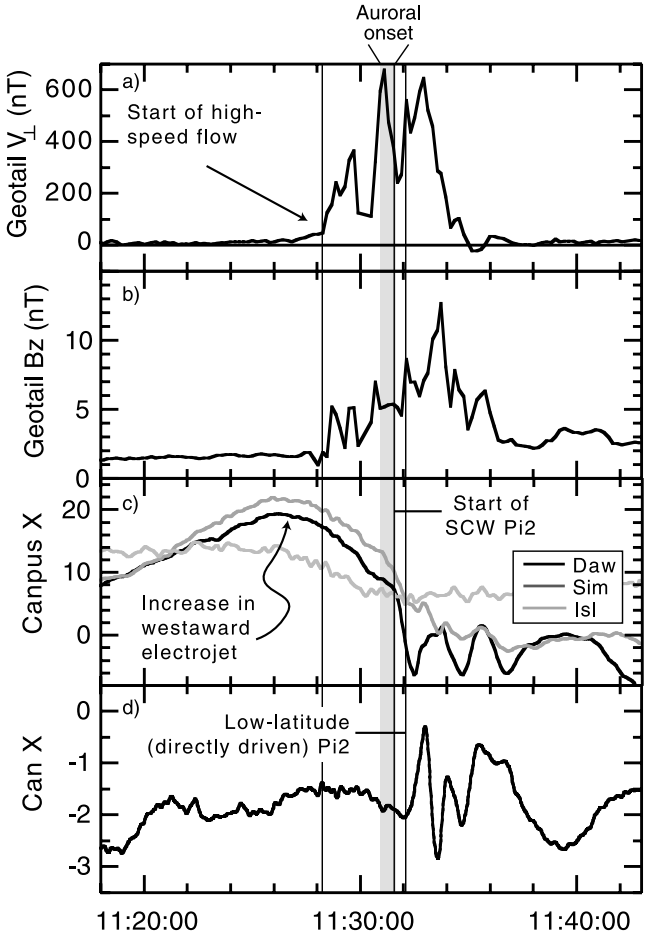

Figure 10. Timing of the October 26, 1997, event. Shown are (a) Earthward component of the perpendicular flow velocity from Geotail; (b) Magnetic field B_z component measured at Geotail; (c) Magnetic H component from nightside, high-latitude stations Daw, Sim and Isl of the Canopus chain; (d) Magnetic X component from low-latitude station Can from the 210MM chain. The time of auroral onset determined from examination of the Polar VIS images is shaded in gray. An increase in the westward electrojet is detected as a decrease in the H component at stations of the Canopus chain starting at 1126 UT. High-speed flow is detected at Geotail a few minutes later just after 1128 UT (first vertical line). Midlatitude Pi2 start at 1131:30 (second vertical line), coincident with auroral arc brightening. Low-latitude Pi2 begin 1 min later (third vertical line).

change in slope represents the onset of substorm current wedge (SCW) pulsations, observable at Dawson, which continued for 2 additional cycles. The shaded box identifies the interval 1130:54-1131:30 UT of a UVI image, which is the most likely interval for discrete auroral arc formation, as discussed previously. Note that the SCW pulsations and the negative bay began in the middle of this time window. In the pre-midnight sector at lower-latitudes Pi2 pulsations observed by Can began ~1 min later, at 1132:15 UT. These Pi2 were at a higher frequency than those observed at Daw and, as we showed previously by *Kepko et al.* [2001], were directly driven by variations in the earthward directed flow in the middle magnetotail.

3. Discussion and Conclusions

[22] While much is well understood in substorm phenomenology, there remains uncertainty as to whether the process initiates close to the Earth and expands tailward (the NGO model) or begins in the near-magnetotail (the NENL model). Event studies are crucial toward a resolution of this topic. In the three events presented in this paper, midtail, convective, Earthward plasma flows preceded auroral onset by 1–3 min. In addition, the onset of nightside Pi2, magnetic bay variations and auroral arc brightening were virtually simultaneous, within the resolution of the auroral images. This latter result contradicts the *Liou et al.* [2000] statistical study that reported a significant delay between nightside Pi2 and auroral arc brightening, an interpretation challenged by *Kepko and McPherron* [2001]. We also showed that the low-latitude, flank Pi2 began within 10s of seconds of the onset of auroral arc formation, nightside, midlatitude Pi2 and nightside bay variations.

[23] In the discussion that follows we use the relative timing of the onset phenomena determined in the previous sections with the correlation of flow and Pi2 waveform presented by *Kepko et al.* [2001] to argue that the initial trigger for activity could not have been located in the near-geosynchronous region. We then show that the onset phenomena are well ordered by the flow-driven model. We also examine the high-latitude magnetic precursor to onset, and identify the currents expected from the passage of a flow burst through the inner plasmasheet prior to substorm onset. Finally, we calculate an analytic expression for this current and show that it is not large enough to generate discrete auroral structures.

[24] According to the NGO models, substorm onset begins with a disruption of the cross-tail current at the inner edge of the tail current sheet. By definition, this current disruption (CD) marks the formation of the substorm current wedge (SCW). This disturbance initiates near the equator and travels along field lines as an Alfvén wave, reaching the auroral zone in 30–60 s. This wave carries intense current and the interaction of the wave with the ionosphere generates auroral arcs and nightside Pi2. As discussed previously, the time of discrete auroral arc formation is commonly used as a marker for substorm onset, even though the instability that initiates that process must start earlier. We know from our observations that low-latitude, flank Pi2 are observed a few tens of seconds later. Although it is unclear how an NGO onset mechanism triggers these Pi2, we assume for the purposes of this discussion that cross-tail current disruption launches a broadband compressional signal into the inner magnetosphere thereby producing Pi2 pulsations. The exact coupling process is unimportant here. The few 10s of seconds delay is the time required for compressional waves to propagate from the source region on the nightside to the flank which is longer than the Alfvénic travel time along field lines to the auroral zone.

[25] We compare the observed relative timing of the onset phenomena with predictions of the NGO model. Although in situ observations of CD were not available, we know that

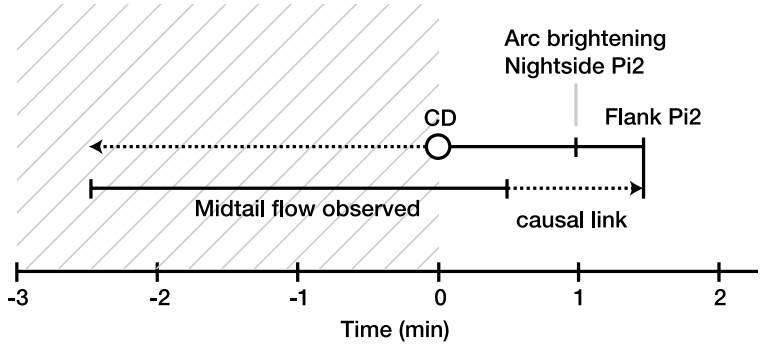

Figure 11. Sequence of onset phenomena determined from the events analyzed in this paper. Midtail plasma flows were observed between 1 and 3 min prior to low-latitude, flank Pi2. They are directly linked by the correlation of flow variation and Pi2 waveform. Auroral arc brightening and nightside Pi2 were observed up to 30 seconds prior to flank Pi2. The inferred time of current disruption (CD), which was not observed, was placed at $T = 0$, 1 min prior to arc brightening and nightside Pi2. The shaded area to the left of $T = 0$ represents times for which CD can have no causal link.

the time from current disruption to arc brightening is the travel time of an Alfvén wave from the near-geosynchronous equator to the ionosphere. This is between 30 and 60 s, depending on the Alfvén speed profile of the inner magnetosphere. We will use an upper limit of 1 min, which corresponds to an average $V_a \sim 800$ km/s. The observed time between arc brightening and the detection of low-latitude Pi2 is <30 s. The combined $\Delta T \leq 90$ s gives an upper limit estimate of the time from current disruption to low-latitude Pi2.

[26] From our observations we know also that midtail flow bursts preceded low-latitude Pi2 by 1–3 min. However, there is the possibility that the observed flows were not directly associated with substorm onset [e.g., *Lyons et al.*, 1999]. To address this question, we use the connection between low-latitude Pi2 pulsations and the flow variations. As we have shown previously [*Kepko and Kivelson*, 1999; *Kepko et al.*, 2001], the time-history of midtail flow variations for these events matched the waveforms of low-latitude Pi2, which were delayed relative to the flow by several minutes. We suggested that this can be explained only if the intermittent compressional waves generated by flow-braking directly drive low-latitude Pi2. This result directly and causally links midtail flow bursts with low-latitude Pi2, for it is the time-variations of the flows themselves that lead to the pulsations. Thus midtail plasma flows cannot be dismissed as being unrelated to the onset phenomena.

[27] We present a timeline of onset phenomena in Figure 11, where we have placed current disruption at epoch time $T = 0$, 1 min prior to nightside Pi2. The relative ordering of the phenomena is based on our observations in this paper. According to the NGO model, CD of the inner current sheet is the trigger for all subsequent onset phenomena. Yet our timing analysis indicates that flows were observed in most cases prior to the inferred time of CD, in a region of the timeline where causality dictates that CD can have no effect (shaded area in Figure 11).

[28] Note that we cannot disassociate the flows from the Pi2; they are linked by the high correlation of flow variations and Pi2 waveforms. In order to salvage the NGO model as a viable mechanism, the onset of CD must be moved several minutes to the left in the timeline, as indicated by the dashed line in Figure 11, to a time at or before the first measurement of Earthward convective flow. This now places the onset of CD up to 3 min before auroral arc brightening, the formation of the SCW, and nightside Pi2 pulsations. In contrast, the maximum time-of-flight for an Alfvén wave from the near-geosynchronous equator is ~1 min. This leads us to one of two possible conclusions. One possibility is that CD, as envisioned in the NGO model, is not directly associated with auroral arc formation, nightside Pi2, or the formation of the SCW. Rather, it is the trigger for convective flows and lies to the far left of the timeline in Figure 11. On the basis of time-of-flight constraints this requires that either the location of CD move further downtail, near the source of the flows, or that near-Earth CD have no measurable impact on the nightside auroral zone. The former scenario takes CD out of the NGO framework while the latter seems physically implausible. The alternative is that CD does not trigger the midtail plasma flows, and that some other process initiates midtail plasma flow well before CD. This option removes near-geosynchronous CD as a viable onset mechanism. In either scenario, the relative timing of onset phenomena for the events presented and analyzed in this study is inconsistent with the NGO model.

[29] We next argue that a phenomenological description that links the initiation of transient convection to other phenomena present in the events presented in this paper clearly support the flow-driven model of magnetospheric dynamics. A schematic version of the model is shown in Figure 12, where we have indicated the substorm-associated currents expected at two different stages of substorm expansion.

[30] The timing analysis of this paper strongly suggests that the first element of substorm expansion is the initiation of high-speed, convective plasma flow in the middle magnetotail. Because of the low probability of having a spacecraft appropriately located to observe the flow, this is not typically the marker used for substorm onset. In this study, the Geotail velocity data were used to identify times of interest thereby providing a number of cases for which both

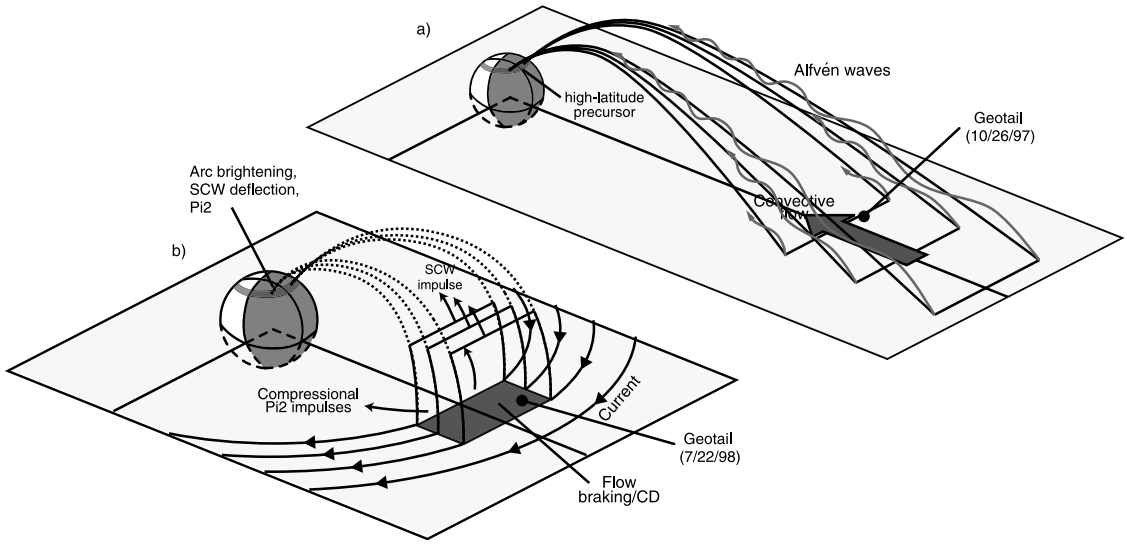

Figure 12. a) The Alfvén waves associated with the initiation of earthward convection. The high-latitude precursor is a response to the total current flowing through the ionosphere, which grows over time as the Alfvén waves reach the ionosphere. The flow continues unimpeded Earthward until it reaches the transition between stretched tail and dipolar field lines, at which point it is braked. This leads to current disruption and the formation of the SCW (b). Discrete auroral arc brightening, nightside Pi2 and strong magnetic bay variations are all direct consequences of the leading edge of the SCW reaching the ionosphere, and are simultaneous. The braking of variable flow launches compressional pulses sunward, leading to low-latitude, flank Pi2.

flow data and auroral data were available. We have found that the flow is the first event in the sequence. From a phenomenological standpoint, it is not important to specify the exact mechanism creating the flow, although magnetic reconnection is most likely. A typical flow burst will travel Earthward at a rate of $\sim 6\ R_E$ per minute. Statistical studies have identified the region $X = -20$ to $X = -30\ R_E$ as the most probable for x-line formation [*Nagai and Machida*, 1998]. Therefore a spacecraft located in the near-Earth plasmasheet will typically detect the flow within 1–2 min of its initiation.

[31] Careful inspection of nightside, high-latitude magnetograms shows a very small negative deflection in the horizontal component (see Figures 3c, 6c, and 10c) at about this same time. Whether this signature appears prior to or after the flow burst is detected in the plasmasheet depends on the position of the spacecraft relative to the location at which the flow originates. For the October 26, 1997 event this deflection was observed before the flow was detected at Geotail, while for the July 22, 1998 event it was observed after the flow was detected. We believe that this deflection, which we have termed the Pi2 precursor, indicates the changed ionospheric convection in the high and midlatitude, near midnight sector that develops when an event in the magnetotail initiates an earthward traveling flow burst. That is, it is a result of the interaction of the Alfvén waves, shown propagating along the field in Figure 12a, with the ionosphere. Noteworthy is that the perturbation of the Pi2 precursor is in the same direction as the perturbation from the substorm current wedge. This suggests that the current system associated with inward convection has the same topology as that caused by current disruption at the tail/dipolar interface. Since the start of the SCW on the ground is simultaneous with the start of the nightside Pi2 and auroral arc brightening, both of which occur after the precursor, the precursor must be a response to processes that occur before the flow reaches the inner magnetosphere; namely, inward convection at larger downtail distance.

[32] We note that the Pi2 precursor is unrelated to the growth phase signature often observed in high-latitude magnetograms [*McPherron*, 1970]. In particular, the growth phase, or DP-2, current system occurs over much longer timescales, 30–60 min, than the 1–3 min duration of the Pi2 precursor. Also, the DP-2 system is a global phenomenon, reflecting the reconfiguration of the magnetosphere in response to changes in convection. In contrast, the Pi2 precursor is highly localized to high-latitudes on the nightside and the width of the signature is expected to relate to the width of the flow channel ($1–3\ R_E$ [*Angelopoulos et al.*, 1996]) in the plasmasheet.

[33] As the flow moves through the plasmasheet, only the Pi2 precursor arises as an ionospheric signature of substorm expansion. This precursor can last a few minutes, its duration depending upon the distance between the flow origin and the braking region, the Alfvén speed profile of the plasmasheet, and the convective velocity of the flow burst. Additional signatures of substorm expansion occur when the flow reaches the inner plasmasheet, where it encounters a rapid increase in magnetic pressure and is slowed. This has been termed "flow-braking" [*Haerendel*, 1992; *Shiokawa et al.*, 1997], and it has two important effects. First, the impact of the flow on the semi-rigid dipolar field lines of the inner magnetosphere launches a fast-mode wave (or a series of fast-mode waves if the flow is oscillatory) that is the source for low-latitude Pi2 pulsations [*Kepko and Kivelson*, 1999; *Kepko et al.*, 2001].

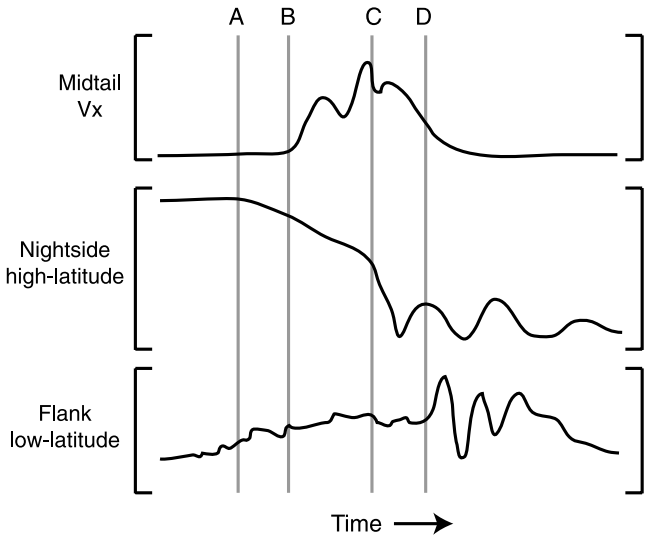

Figure 13. The signatures expected at a midtail spacecraft located in the plasmasheet (top), high-latitude ground station (middle), and a low-latitude, flank ground station (bottom). Vertical lines mark times for: Pi2 precursor observed at high-latitude ground station (A); Midtail plasma flow observed (B); Arrival of leading edge of SCW current at the ionosphere (C); low-latitude, flank Pi2 (D).

Second, the azimuthal pressure gradients and magnetic shear generated by the interaction cause the substorm current wedge to form and disrupt the cross-tail current [see, e.g., *Birn and Hesse*, 1996]. A spacecraft located in the CD region would measure severe turbulence of the magnetic field followed by a rapid dipolarization of magnetic field lines [e.g., *Lui*, 1996]. This is illustrated in Figure 12b. Geotail was located in the braking region for the July 22, 1998 event, as indicated by both the rapid dipolarization immediately after the first detection of flow and the relatively brief delay between flow detection and auroral signatures (30 s). Compare, for example, the data for the October 26, 1997 event in which Geotail was located further downtail. For that event no local dipolarization occurred, and the auroral signatures occurred 3 min after flow was first observed.

[34] The SCW is the principle driver of substorm-associated nightside ground and auroral phenomena. The leading edge of the Alfvén wave associated with the initiation of the current will take ~1 min to reach the ionosphere. Because of the impedance mismatch between the ionosphere and the auroral flux tubes, a fraction of this current is reflected. This is the well-known transient-response mechanism (see review by *Baumjohann and Glaßmeier* [1984]) for nightside, midlatitude Pi2 pulsations, which we have termed SCW Pi2 [*Kepko et al.*, 2001] to emphasize the source. The sudden surge in current, up to $\sim 10^6$ amps, exceeds the capacity of the ionosphere to passively respond, so intense field-aligned potential drops develop on the westward edge of the SCW. The downward acceleration of electrons into the ionosphere generates the discrete arcs. The intensification of discrete arcs is commonly referred to as "auroral onset". Note that in this scenario the sudden change in the horizontal components of the field in ground magnetograms close to the leading edge of the SCW current in the ionosphere, the initial SCW Pi2 deflection and the auroral arc brightening are simultaneous, as required by the observations. Low-latitude, flank Pi2 follow a few tens of seconds later. The delay is due to the different path (perpendicular to magnetic field lines) along which the flow braking-generated waves must travel [see *Kepko and Kivelson*, 1999].

[35] We show in Figure 13 idealized observations expected from the scenario described above. At top we show the convective flow velocity measurements from a satellite in the midtail plasmasheet, followed by the *H* component magnetic field perturbation measured at a high-latitude ground station (middle), and the *H* component Pi2 signature observed at low-latitude on the flank (bottom). All of these signatures have been modeled after the October 26, 1996 event (compare with Figure 10), but the characteristics are general. In summary (Figure 13):

[36] 1. If convective flow starts well tailward of the midtail location of the spacecraft, Alfvén waves launched at the start of the flow disturbance may reach the ionosphere before the flow arrives at the spacecraft. In such cases (illustrated here) the first indication of the initiation of transient convection is a slight deflection in high-latitude *H* component magnetograms (A).

[37] 2. Within a few minutes high-speed, convective, Earthward plasma flow is observed in the plasmasheet (B). When the flow reaches the transition between stretched tail and dipolar field lines it is braked, creating the SCW wedge and CD. This flow braking also launches fast-mode waves sunward, with the same periodicity as the flow variations.

[38] 3. The interaction of the SCW with the ionosphere causes discrete auroral arcs to intensify, generates midlatitude Pi2s, and produces a sharp decrease in the horizontal magnetic field (C).

[39] 4. Within a few 10s of seconds, the fast-mode waves associated with flow braking directly drive flank, low-latitude Pi2 (D).

[40] The events studied in this paper ranged from a moderate substorm (the July 22, 1998 event where *AL* reached −200 nT) to a small, highly localized minor breakup (the October 26, 1997 event). Despite the very different levels of activity in the three events, the onset phenomena changed only in magnitude, not in their temporal order. We believe that this indicates that small-scale flow bursts, pseudobreakups and substorms can be classified generally as fundamental units of transient convection that differ only in magnitude, not in underlying physics.

[41] Several works have suggested that the lack of observable auroral activity prior to auroral onset is incompatible with the flow-driven model [e.g., *Liou et al.*, 1999]. Our analysis has identified a weak ionospheric precursor to auroral onset in the form of a small magnetic perturbation at high-latitude, which we have termed the Pi2 precursor. We have argued that this is the signature of an ionospheric current that we have attributed to the Earthward motion of a magnetotail flow burst. Yet it is not immediately apparent why this precursor current does not appear to drive auroral activity. We now derive an analytical expression relating the ionospheric current to an incoming flow burst and estimate the magnitude of the associated current. We show that the expected current

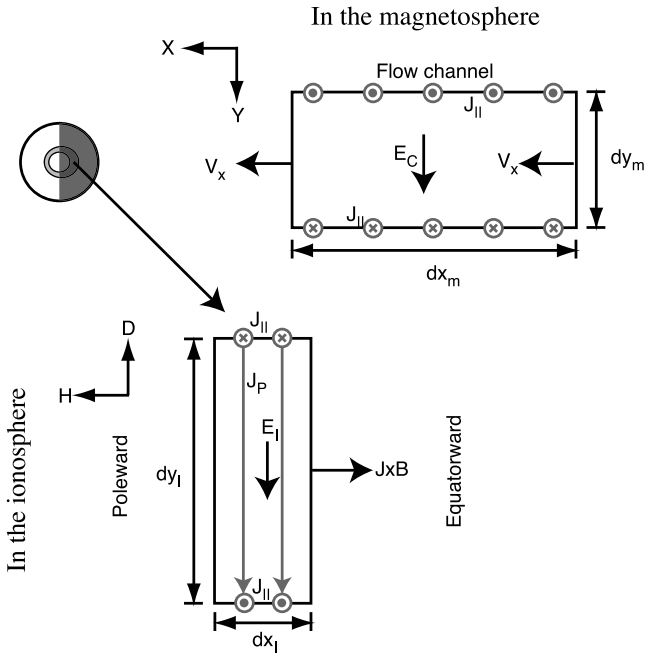

Figure 14. Schematic showing the electric fields, currents, and dimensions in the magnetosphere and ionosphere associated with an earthward travelling flow burst. In the magnetosphere a flow burst with length dx_m propagates earthward with velocity V_x. The convective electric field (E_0) is applied to the ionosphere where it drives a Pedersen current which provides the $\mathbf{J} \times \mathbf{B}$ force necessary to move the ionospheric footprint equatorward.

flowing into the ionosphere is quite small compared to typical SCW currents. We then argue that these currents are too small to generate the intense parallel electric fields necessary for discrete auroral arc formation.

[42] In the magnetosphere we assume a flow channel with total radial extent dx_m and an east-west width of dy_m (Figure 14). The flow propagates earthward with velocity V_x, and has an associated convection electric field, $\mathbf{E_c} = -\mathbf{V} \times \mathbf{B}$, which points in the direction from dawn to dusk. Here $\mathbf{B}$ is the northward directed ambient magnetic field in the central plasma sheet. At the edges of the flow channel field-aligned currents flow into (at dusk) and away from (at dawn) the ionosphere. Note that this current is in the same sense as the SCW, and produces perturbations in the same direction as those observed in this paper. The convective electric field of the flow burst projects onto the ionosphere where it drives a Pedersen current that contributes the $\mathbf{J} \times \mathbf{B}$ force acting to move the ionospheric footprint equatorward. The linear Pedersen current density, j_p, in units of amps/m is

$$j_P = \Sigma_P E_I. \tag{1}$$

Here Σ_P is the height integrated Pedersen conductivity (mhos) and E_I is the ionospheric electric field (V/m), related to the convective electric field E_c in the tail by a geometric scaling factor (assuming no parallel potential drops). Note that the cross-product of j_P with the ambient magnetic field is equatorward. The total perturbation current flowing in the ionosphere, I_p, is the integral of (1) over the latitudinal (north-south) projection of the channel, such that

$$I_P = \Sigma_P E_I dx_I, \tag{2}$$

where dx_I is the north-south width of the current, which is simply the projection of the radial length of the flow channel (dx_M) onto the ionosphere. Note that dx_M (and therefore dx_I) is in principle a time dependent quantity, though we will not treat it is as such in this order of magnitude estimate.

[43] Assuming no field-aligned potential drops, the total potential drop across the flow channel equals the potential drop across the width of the channel projected onto the ionosphere, dy_I. The relation

$$E_C dy_M = E_I dy_I \tag{3}$$

shows that the scaling factor that relates the ionospheric electric field to the convective electric field is dy_M/dy_I. Equation (2) now becomes

$$I_P = \Sigma_P V_{flow} B_{tail} \frac{dy_M}{dy_I} dx_I. \tag{4}$$

[44] We can calculate the current flowing through the ionosphere. Using upper limit estimates of $\Sigma_P = 10$ mhos, $V_{flow} = 1000$ km/s, $B_{tail} = 10$ nT, $dy_M = 2\ R_E$, $dy_I = 1500$ km, and $dx_I = 200$ km, we obtain $I_P < 10^5$ amps, which is an order of magnitude lower than the typical substorm current wedge magnitude of 10^6 amps. We note that more realistic values of Σ_P, V_{flow}, and B_{tail} reduce this estimate by an order of magnitude, to 10^4 amps. Directly beneath this ionospheric current the magnetic perturbation would be a few tens of nanoteslas, consistent with the observations in this paper. Further equatorward, midlatitude magnetometer stations would measure perturbations due to the field-aligned section of this current system. The perturbation at these stations is typically reduced by a factor of 10–20 compared to measurements directly beneath the current. Our observations indicate that the precursor is <20 nT at high-latitude stations, consistent with our crude estimate.

[45] Although crude, our calculations show that the current flowing through the ionosphere prior to auroral onset is quite small compared to the SCW current. Parallel electric field is called for only for relatively large currents. It is because the SCW current is upward of 1 MA that the parallel electric fields that generate the discrete aurora are required in order to drive electrons downward. These parallel electric fields seem not to be needed to produce the smaller Pi2 precursor currents, because no discrete arcs form. We do not argue that there should be no optical ionospheric signature. Rather, we suggest that this signature is too weak to have been observed.

[46] We note that in a few instances observable auroral features have been linked to plasmasheet flows. These features, termed "auroral streamers", occur first at the high-latitude auroral zone boundary and then move equatorward [*Lyons et al.*, 1999; *Zesta et al.*, 2000; *Nakamura et al.*, 2001]. The flows associated with the streamers occur most often tailward of $X = -15\ R_E$ during substorm recovery phase when the plasmasheet is relatively thick [*Nakamura et al.*, 2001]. In contrast, the events presented here occurred Earthward of $X = -15\ R_E$ and were closely linked with substorm onset and poleward expansion of the

aurora. The difference in plasmasheet configuration between near-Earth flows associated with onset versus those that occur further downtail during the recovery phase likely accounts for the different auroral signatures of the two types of flows. *Nakamura et al.* [2001] studied both types of events and concluded that the flows associated with auroral streamers experience stronger flow shear due to the dipolar configuration of the middle plasmasheet, thus producing increased field-aligned currents.

[47] **Acknowledgments.** Most of this work was performed while L. Kepko was still a graduate student at UCLA. As such, he is indebted to all of his UCLA friends and colleagues who provided help and insight. In addition we thank S. Kokubun and T. Mukai for Geotail magnetic field and plasma data, which were obtained through DARTS at the Institute of Space and Astronautical Science (ISAS) in Japan. Polar VIS and UVI images were obtained from CDAWeb and were provided by L. Frank and G. Parks, respectively. That CANOPUS instrument array was constructed and is maintained by the Canadian Space Agency. The Los Alamos magnetic field data were obtained from the UCLA data server at http://www-ssc.igpp.ucla.edu/uclamag/data_center/. 210°MM data were provided by K. Yumoto. This paper was prepared with partial support from Los Alamos National Laboratory under IGPP grant 31113 and from the National Science Foundation under ATM 02-05958. UCLA Institute of Geophysics and Planetary Physics Publication 5809.

[48] Arthur Richmond thanks Wolfgang Baumjohann and Tsugunobu Nagai for their assistance in evaluating this paper.

References

Akasofu, S.-I. (1964), The development of the auroral substorm, *Planet. Space Sci.*, *12*, 273–282.

Angelopoulos, V., et al. (1996), Multipoint analysis of a bursty bulk flow event on April 11, 1985, *J. Geophys. Res.*, *101*, 4966–4990.

Baker, D. N., T. I. Pulkkinen, V. Angelopoulos, W. Baumjohann, and R. L. McPherron (1996), Neutral line model of substorms: Past results and present view, *J. Geophys. Res.*, *101*, 12,975–13,010.

Baumjohann, W., and K.-H. Glaßmeier (1984), The transient response mechanism and Pi2 pulsations at substorm onset: Review and outlook, *Planet. Space Sci.*, *32*, 1361–1370.

Baumjohann, W., M. Hesse, S. Kokubun, T. Mukai, T. Nagai, and A. A. Petrukovich (1999), Substorm dipolarization and recovery, *J. Geophys. Res.*, *104*, 24,995–25,000.

Birn, J., and M. Hesse (1996), Details of current disruption and diversion in simulations of magnetotail dynamics, *J. Geophys. Res.*, *101*, 15,345–15,358.

Birn, J., M. Hesse, G. Haerendel, W. Baumjohann, and K. Shiokawa (1999), Flow braking and the substorm current wedge, *J. Geophys. Res.*, *104*, 19,895–19,904.

Frank, L. A., J. B. Sigwarth, J. D. Craven, J. P. Cravens, J. S. Dolan, M. R. Dvorsky, P. K. Hardebeck, J. D. Harvey, and D. W. Muller (1995), The Visible Imagining System (VIS) for the Polar spacecraft, *Space Sci. Rev.*, *71*, 297–328.

Haerendel, G. (1992), Disruption, ballooning or auroral avalanche—On the cause of substorms, paper presented at First International Conference on Substorms (ICS-1), Eur. Space Agency, Kiruna, Sweden.

Kepko, L., and M. G. Kivelson (1999), Generation of Pi2 pulsations by bursty bulk flows, *J. Geophys. Res.*, *104*, 25,021–25,034.

Kepko, L., and R. L. McPherron (2001), Comment on "Evaluation of low-latitude Pi2 pulsations as indicators of substorm onset using Polar ultraviolet imagery" by K. Liou et al., *J. Geophys. Res.*, *106*, 18,919–18,922.

Kepko, L., M. G. Kivelson, and K. Yumoto (2001), Flow bursts, braking, and Pi2 pulsations, *J. Geophys. Res.*, *106*, 1903–1915.

Kokubun, S., T. Yamamoto, M. H. Acuna, K. Hayashi, K. Shiokawa, and H. Kawano (1994), The Geotail Magnetic Field Experiment, *J. Geomagn. Geoelectr.*, *46*, 7–21.

Liou, K., C.-I. Meng, A. T. Y. Lui, P. T. Newell, M. Brittnacher, G. Parks, G. D. Reeves, R. R. Anderson, and K. Yumoto (1999), On relative timing in substorm onset signatures, *J. Geophys. Res.*, *104*, 22,807–22,817.

Liou, K., C.-I. Meng, P. T. Newell, K. Takahashi, S.-I. Ohtani, A. T. Y. Lui, M. Brittnacher, and G. Parks (2000), Evaluation of low-latitude Pi2 pulsations as indicators of substorm onset using Polar ultraviolet imagery, *J. Geophys. Res.*, *105*, 2495–2505.

Lui, A. T. Y. (1996), Current disruption in the Earth's magnetosphere: Observations and models, *J. Geophys. Res.*, *101*, 13,067–13,088.

Lyons, L. R., T. Nagai, G. T. Blanchard, J. C. Samson, T. Yamamoto, T. Mukai, A. Nishida, and S. Kokubun (1999), Association between Geotail plasma flows and auroral poleward boundary intensifications observed by CANOPUS photometers, *J. Geophys. Res.*, *104*, 4485–4500.

McPherron, R. L. (1970), Growth phase of magnetospheric substorms, *J. Geophys. Res.*, *75*, 5592–5599.

Mukai, T., S. Machida, Y. Saito, M. Hirahara, T. Terasawa, N. Kaya, T. Obara, M. Ejiri, and A. Nishida (1994), The low energy particle (LEP) experiment onboard the Geotail satellite, *J. Geomagn. Geoelectr.*, *46*, 669–692.

Nagai, T., and S. Machida (1998), Magnetic reconnection in the near-earth magnetotail, in *New Perspectives on the Earth's Magnetotail*, *Geophys. Monogr. Ser.*, vol. 105, edited by A. Nishida, D. N. Baker, and S. W. H. Cowley, pp. 211–224, AGU, Washington, D. C.

Nakamura, R., W. Baumjohann, R. Schëdel, M. Brittnacher, V. A. Sergeev, M. Kubyshkina, T. Mukai, and K. I. Liou (2001), Earthward flow bursts, auroral streamers, and small expansions, *J. Geophys. Res.*, *106*, 10,791–10,802.

Shiokawa, K., W. Baumjohann, and G. Haerendel (1997), Braking of high-speed flows in the near-Earth tail, *Geophys. Res. Lett.*, *24*, 1179–1182.

Shiokawa, K., et al. (1998), High-speed ion flow, substorm current wedge, and multiple Pi2 pulsations, *J. Geophys. Res.*, *103*, 4491–4508.

Torr, M. R., et al. (1995), A far ultraviolet imager for the International Solar Terrestrial Physics Mission, *Space Sci. Rev.*, *71*, 329–383.

Tsyganenko, N. A. (1989), A magnetospheric magnetic field model with a warped tail current sheet, *Planet. Space Sci.*, *37*, 5–20.

Yumoto, K., and the 210 (deg) M Magnetic Observation Group (1996), The STEP 210 (deg) magnetic meridian network project, *J. Geomagn. Geoelectr.*, *48*, 1297–1309.

Zesta, E., L. Lyons, and E. Donovan (2000), The auroral signature of earthward flow bursts observed in the magnetotail, *Geophys. Res. Lett.*, *27*, 3241–3244.

L. Kepko and H. E. Spence, Center for Space Physics, Boston University, 725 Commonwealth Avenue, Boston, MA 02215, USA. (lkepko@bu.edu)

M. G. Kivelson and R. L. McPherron, Institute of Geophysics and Planetary Physics, University of California, Los Angeles, Los Angeles, CA 90024, USA. (mkivelson@igpp.ucla.edu; mcpherron@igpp.ucla.edu)

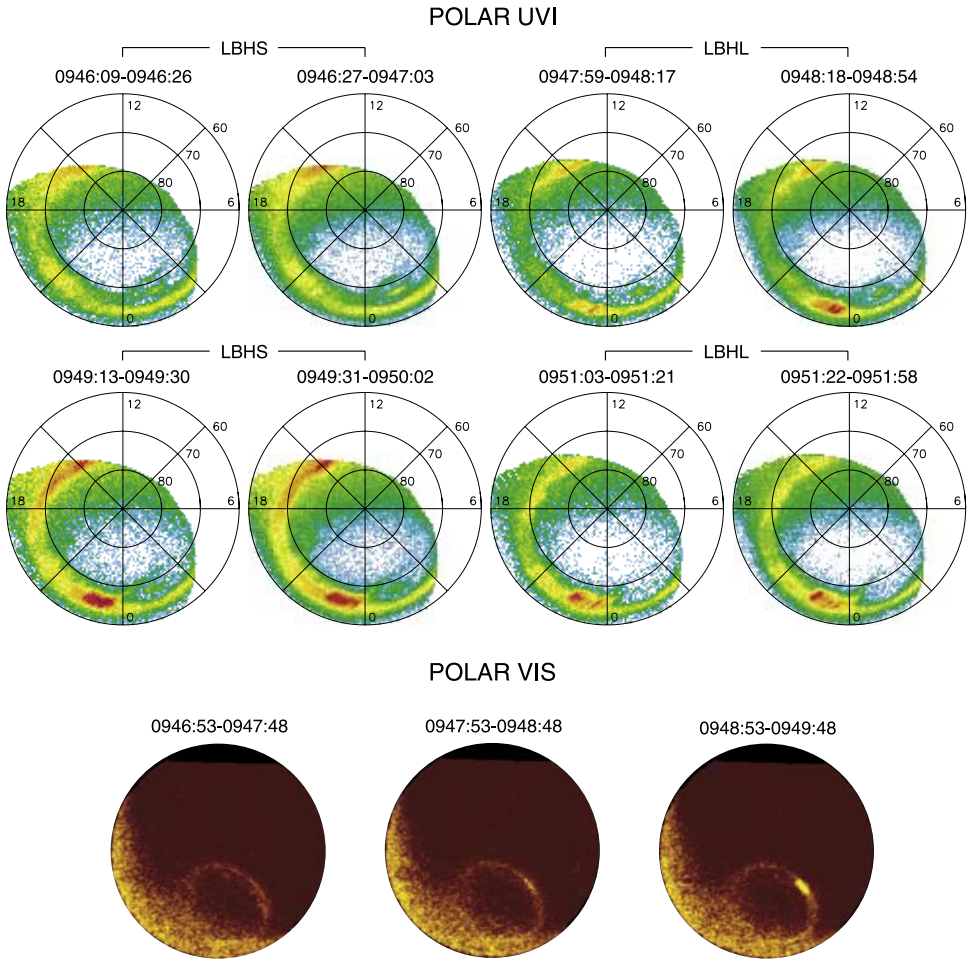

Figure 2. Images from the Polar UVI (rows 1 and 2) and VIS (row 3) for the September 4, 1997 event. The first indication of auroral brightening is observed in the 0947:59-0948:17 UVI image. Later images show that this arc intensifies and expands. In all VIS images, diffuse brightness at latitudes equatorward of the auroral oval occurs in sunlit regions and identifies dayside local times.

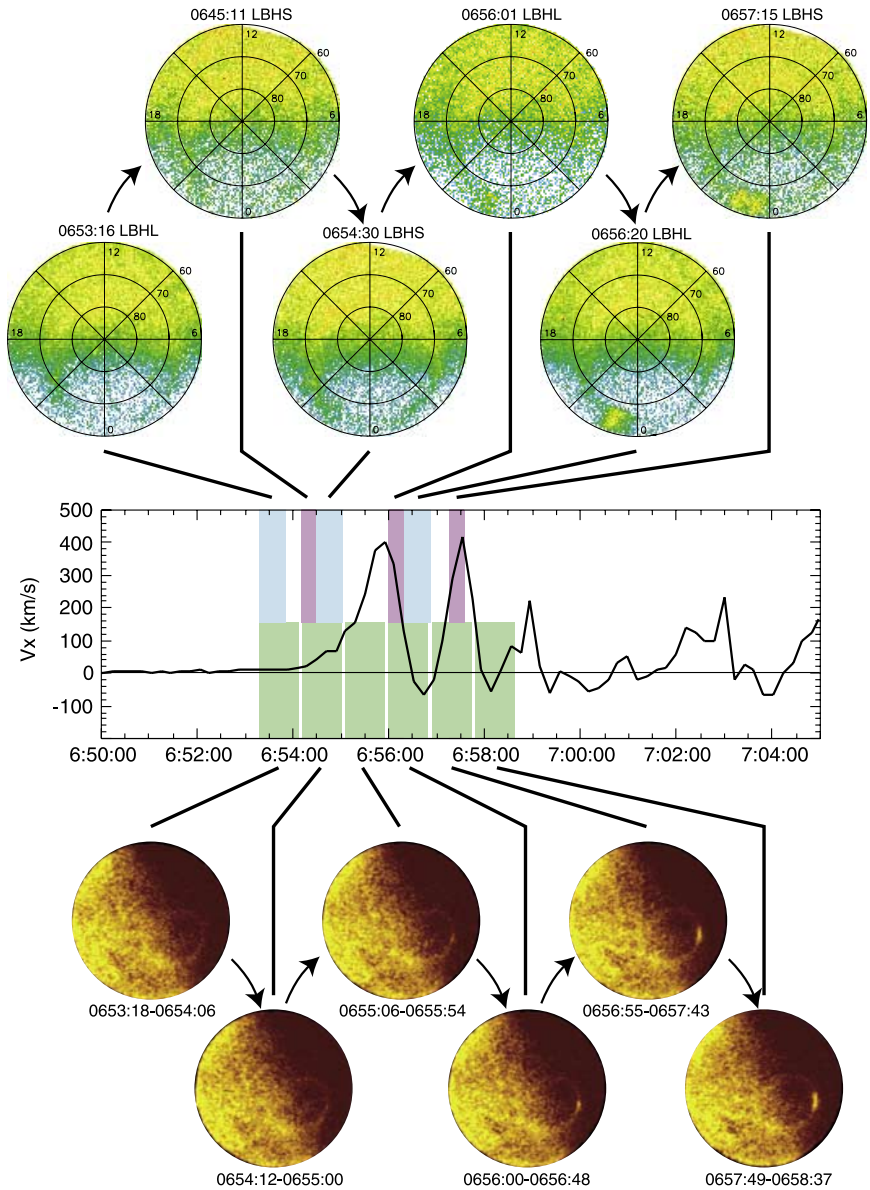

Figure 5. Auroral images from the UVI (top) and VIS (bottom) from Polar for the July 22, 1998, event. Detailed descriptions of the images are given in the text. Also shown (middle) are the flow data from Geotail. Shaded boxes indicate integration periods for each image.

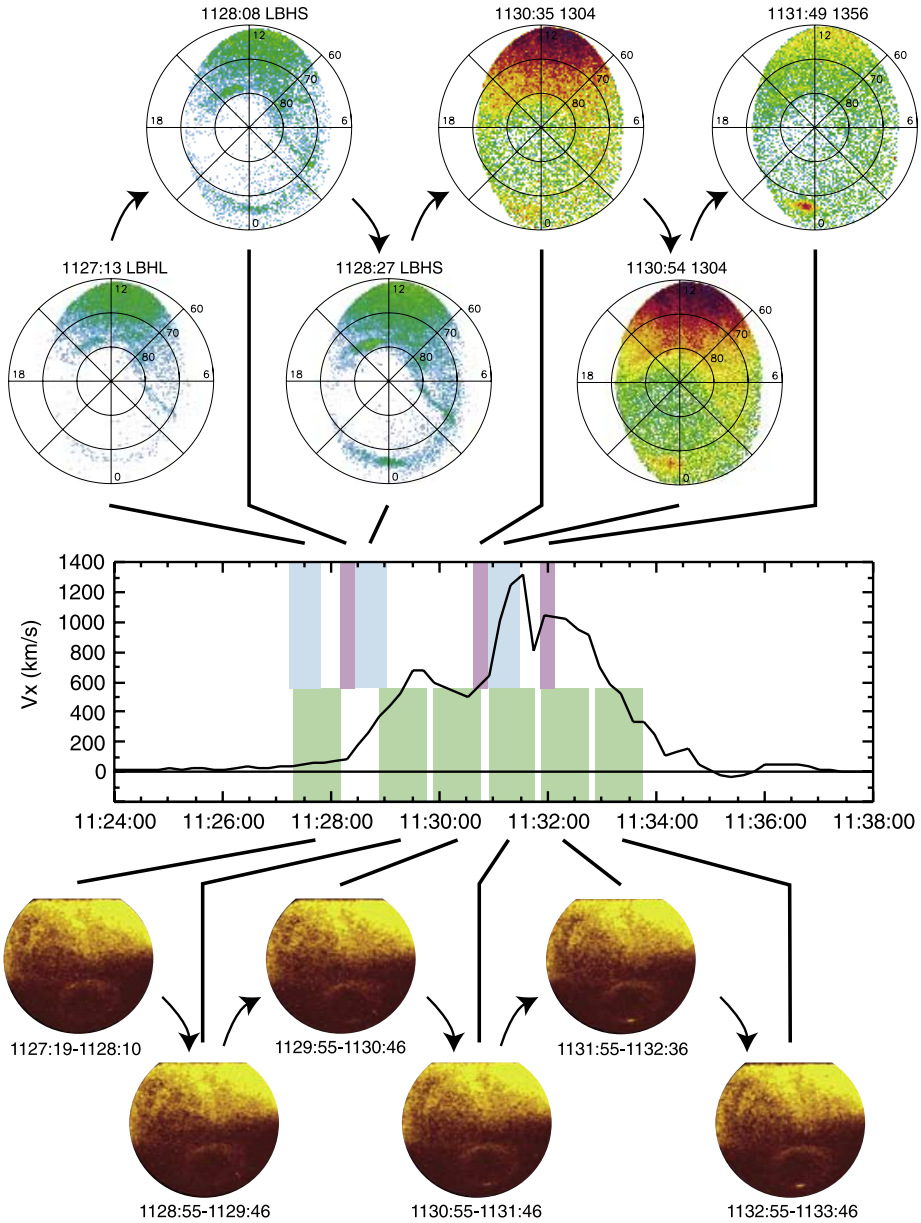

Figure 8. Images from the Polar UVI (top) and VIS (bottom) auroral imagers for the October 26, 1997, event. Also shown (middle) are the flow data from Geotail. Shaded boxes identify integration periods for each auroral image.

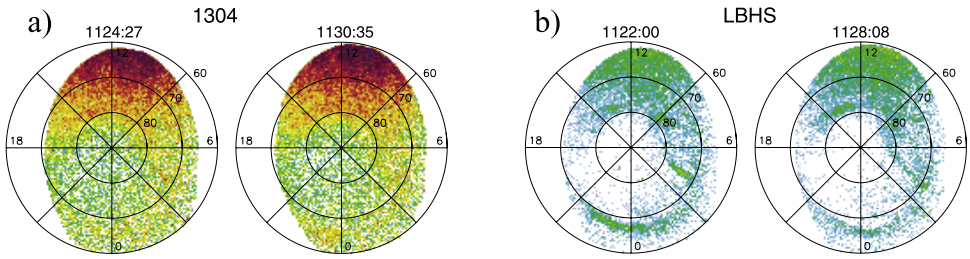

Figure 9. Comparison of pairs of a) 1304 and b) LBHS images taken ~6 min apart by the UVI on board Polar.